Bulletin of the JSME Vol.14, No.2, 2019
Journal of Fluid Science and Technology

Shear stress fluctuation measurements using an electrochemical method in pipe flow

Tong TONG *, Tatsuya TSUNEYOSHI * and Yoshiyuki TSUJI*
* Department of Energy Engineering and Science, Nagoya University
Furo-cho, Chikusa-ku, Nagoya, Aichi, 464-8601, Japan
E-mail: c42406a@nucc.cc.nagoya-u.ac.jp

Received: 20 September 2019; Accepted: 30 October 2019

Abstract
Wall shear stress fluctuations are measured using an electrochemical method in pipe flow. The relationship between the mass transfer and the momentum transfer, studied by Hanratty and Campbell (1983) and the Chilton–Colburn analogy (Chilton and Colburn, 1934), are compared to each other with respect to the mean wall shear stress and the wall shear stress fluctuation. Chilton–Colburn analogy has been applied to measure the mean wall shear stress in the fully developed concentration boundary layer. There are few studies concerning the feasibility of the Chilton–Colburn analogy for instantaneous wall shear stress measurements. In the present study, with the new designed overall electrode, the feasibility of Chilton–Colburn analogy for predicting the wall shear stress fluctuations is studied for the first time. The friction factor is used to compare the mean wall shear stresses. It is found that both methods can accurately predict the mean wall shear stress. The wall shear stress fluctuations are compared via the probability density function and frequency spectrum. When the probability density fluctuation is normalized by the standard deviation and the spectrum is normalized by the typical time scale, these two methods show the similar statistical properties. It is confirmed that with the new designed overall electrode, Chilton–Colburn analogy is available for predicting the wall shear stress fluctuations.

Keywords : Wall shear stress fluctuation, Chilton–Colburn analogy, Electrochemical method, Pipe flow, Simultaneous measurement

1. Introduction

The detailed structures of the fluctuating turbulent shear flow in the near wall region are extremely important. From the engineering point of view, the mean wall shear stress has an importance since it is associated with the sources of energy dissipation (drag). Additionally, in wall-bounded flows, the experiments (Alfredsson et al., 1988; Marusic et al., 2007) and numerical simulations (Örlü and Schlatter, 2011) found that very large fluctuations of wall shear stress can occur well above the mean values. Such large amplitudes of wall shear stress fluctuations are important for wall-thinning (or FAC: flow accelerated corrosion). FAC is enhanced by the interaction between the wall shear stress and concentration boundary layer (Shan, 2014). From the view of physics, the instantaneous distribution of the shear stress is signatures of the coherent structures occurring above the wall. For example, statistically, the footprints of the near-wall streaks are clearly visible in wall shear stress (Hutchins et al., 2011). Additionally, the imprint of the large-scale structures in log-region is as a modulation of the wall shear stress (Schlatter and Örlü, 2010).

Several techniques for measuring the wall shear stress have been studied. In general, these techniques are separated into two main categories: direct and indirect methods. As a direct method, floating-element sensors are the simplest devices available to measure the instantaneous wall shear stress (Winter, 1979). Indirect methods used for shear stress measurements include the momentum integral equation and the use of similarities between several turbulent quantities. In such indirect methods, the von Karman integral method (White and Frank, 2005), the Clauser plot method (Clauser, 1954), and the Preston tube (Patel, 1965) are used to measure the mean wall shear stress. Using the similarities between

Paper No.19-00456
[DOI: 10.1299/jfst.2019jfst0013]

the wall shear stress and other transfer quantities in the near wall region, the instantaneous wall shear stress can be measured via a hot wire (Sandborn, 1979) or hot film (Sumer et al., 1993) and electrochemical mass transfer probes (Mitchell and Hanratty, 1966). In the present study, we take advantage of the similarities between the mass transfer and the momentum to make instantaneous wall shear stress measurements using an electrochemical method. There are two methods for establishing the relationship between the wall shear stress and the mass transfer rate: one is a method developed by Hanratty and Campbell (1983) and the other is according to the Chilton–Colburn analogy (Chilton and Colburn, 1934).

Under several assumptions, Mitchell and Hanratty (1966) showed how electrochemical mass transfer probes can be used to study the time-averaged and instantaneous wall shear stress for a turbulent flow and pointed out the need to account for spatial averaging and for the time response of the concentration boundary layer. Hanratty and Campbell (1983) gave a summary of the experimental and theoretical problems associated with this technique for measuring the instantaneous wall shear stress. In their study, they provided a solution of the mass balance equation for a steady flow. Based on their study, it is possible to measure the instantaneous wall shear stress in various flow fields. However, the use of this equation has been limited to flows with small amplitude oscillations, owing to the capacitance effect of the concentration boundary layer over the electrode (Fortuna and Hanratty, 1971). There are few studies focusing on measurements of the instantaneous wall shear stress.

Under the condition of a fully developed concentration profile, Chilton and Colburn (1934) predicted the mass transfer rate using the heat transfer and the fluid friction. Lin et al. (1951) applied the Chilton–Colburn analogy between the mass transfer and the fluid friction to verify the average mass transfer rate measured using an electrochemical method in turbulence. The agreement between the data and the Chilton–Colburn analogy was within the deviation of ± 4.9%. Chin and Hsueh (1986) used an electrochemical method to measure the average mass transfer rate on a flat surface from an unsubmerged circular impinging jet, and the Chilton–Colburn analogy has also been used to compare the mass transfer characteristics in the impingement and boundary layer regimes to theoretical predictions. Silverman (2005) provided a relationship between the mean wall shear stress and the mass transfer rate for a rotating cylindrical electrode using the Chilton–Colburn analogy. The Chilton–Coburn analogy is associated with the mass transfer, heat transfer, and momentum in turbulence on comparing with the study by Hanratty and Campbell (1983). However, the Chilton–Colburn analogy needs to be used under a fully developed concentration profile and is primarily applied to mean wall shear stress measurements.

In electrochemical method, the electrode should be long enough to generate a fully developed concentration boundary layer. However, if we use the long electrode for the measurement, the attenuation of the signal averaged over the electrode surface is not negligible for the measurement of fluctuations. Therefore, it might be difficult to predict the wall shear stress fluctuations by way of Chilton–Colburn analogy with the long electrode. Due to the limitation of long electrode setting in the concentration boundary layer, there are few studies concerning verifications confirming the application of the Chilton–Colburn analogy for instantaneous wall shear stress measurements.

As mentioned above, for wall shear stress measurements using electrochemical methods, there are two relationships between the mass transfer rate and the wall shear stress that correspond to the method of Hanratty (Hanratty and Campbell, 1983) and the Chilton–Colburn analogy. And these relationships can be satisfied to predict the time-averaged wall shear stress. However, a comparison between these two methods with respect to predicting the mean wall shear stress has not yet been made. For wall shear stress fluctuation measurements, Hanratty and his coworkers studied flows with small amplitude oscillations. However, there are few studies verifying predictions of wall shear stress fluctuations using the Chilton–Colburn analogy. Therefore, in the present study, to measure the instantaneous wall shear stress in pipe flow, two types of electrodes are utilized: a point electrode and our new design, called overall electrode, corresponding to the method of Hanratty and Campbell (1983) and the Chilton–Colburn analogy (Chilton and Colburn, 1934), respectively. For the point electrode, a single circular electrode with a diameter of 1 mm is isolated and flush mounted on the pipe wall and then the concentration boundary layer is developed only on the small surface of the electrode. For the overall electrode, even though the mass transfer rate is measured by the isolated, flush-mounted point electrode, the concentration boundary layer is fully developed not only over the point electrode surface but also over the entire wall surface.

This study is threefold. First, the mean wall shear stress predictions resulting from the method of Hanratty and Campbell (1983) and the Chilton–Colburn analogy are compared. Second, the feasibility of the Chilton–Colburn analogy for predicting the shear stress fluctuation using the new designed overall electrode is verified. Third, regarding

[DOI: 10.1299/jfst.2019jfst0013]

the point electrode, the spatial resolution effect of the present experiment is studied with the help of direct numerical simulation (DNS) data calculated for the channel flow (Mehrez et al., 2019).

2. Experimental apparatus and methods

In this study, the wall shear stress is calculated from the mass transfer rate, which is measured via an electrochemical method. We believe that this electrochemical method is one possible way to measure the wall shear stress without abruptly changing the hydrodynamic conditions via the connection between the electrodes and the pipe wall. The instantaneous wall shear stress is indicated by $\widetilde{\tau_w}$ and the mass transfer rate is $\tilde{k}$. These quantities are defined by their means and fluctuations as follows: $\widetilde{\tau_w} = \overline{\tau_w} + \tau_w'$ and $\tilde{k} = \bar{k} + k'$.

2.1 Electrochemical method for the mass transfer rate

Figure 1(a) shows the experimental loop for the mass transfer measurement. The electrolytic solution in the tank is circulated through the pipe via a pump. To obtain a fully developed turbulent state, the distance from the pump to the test section is set to 75 D, based on the pipe diameter D = 40 mm.

In this study, to measure the mass transfer rate, we use a three-electrode system (Bard et al., 1980), as shown in Fig. 1 (b), which consists of a cathode (as working electrode, WE), an anode (as counter electrode, CE), and a reference electrode (RE). The working electrode, which contacts the analyte, acts as the cathode. It is necessary to apply a desired potential in a controlled way to facilitate the transfer of charge from the analyte. The counter electrode acts as the anode and requires a known potential to balance the charge added or removed by the working electrode. It is extremely difficult for the counter electrode to maintain a constant potential while, at the same time, passing the current to counter redox events at the working electrode. To solve this problem, the reference electrode is used as an anode with a known reduction potential. Its only use is to act as reference when measuring and controlling the potential of the working electrode; it does not pass any current. In the present experiment, the test section made of a nickel pipe, which is embedded with nickel electrodes, is as long as 5 D. To ensure that the current flowing into the circuit is controlled by reactions at the working electrode surface, nickel pipes with large lengths are used as counter electrodes and are located upstream and downstream of the test section. The lengths of the counter electrodes are 25 D (upstream) and 7 D (downstream). The reference electrode is located in the test section as shown in Fig. 1(a).

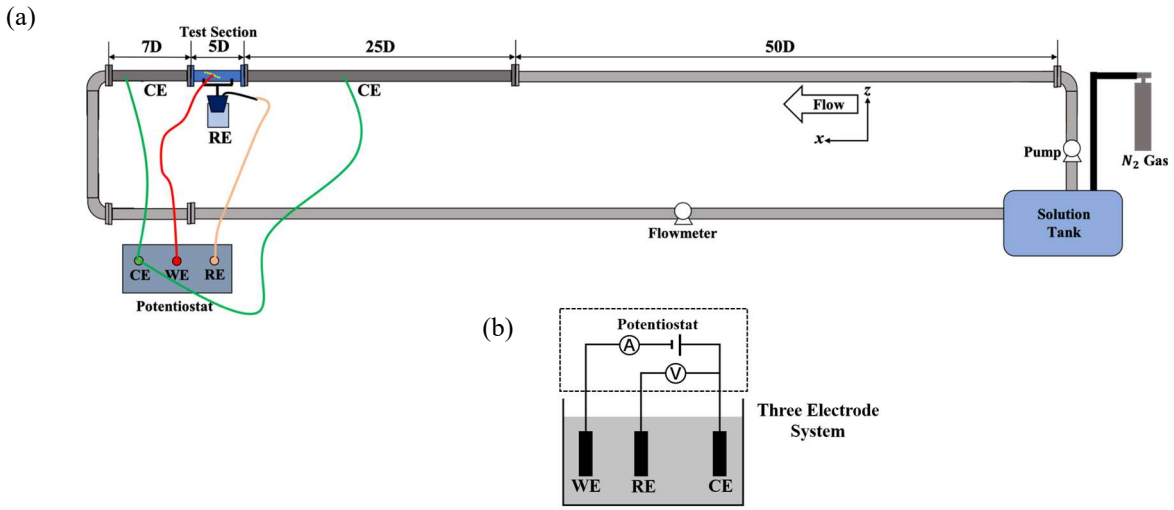

Fig. 1 (a) Schematic view of the experimental apparatus for the mass transfer measurement. (b) The three-electrode setup: working electrode (WE); counter electrode (CE); and reference electrode (RE).

In the test section, to prevent the effect of the concentration boundary layer developed by the upstream electrode on the adjacent downstream electrode, eight working electrodes are arranged spirally along the pipe. The angle between each electrode is 10° in the pipe cross-section, and the distance between each electrode is 0.4 R along the pipe streamwise, as shown in Fig. 2 (a). The suffix "ch" is used to denote the position of the working electrodes. The working electrodes are also made of nickel, are 1 mm in diameter, and are mounted on the pipe surface. The electrodes

[DOI: 10.1299/jfst.2019jfst0013]

are isolated against the pipe wall with a distance of 0.3 mm. Acrylic resin is used as an isolating layer.

The electrolytic solutions, which are used to measure the mass transfer rates in this study, are redox couples of ferrocyanide and ferricyanide ions with a concentration of $0.25\ \mathrm{mol/m^3}$ and K_2SO_4 as an unreactive electrolyte. The reactions in these systems are

$Fe(CN)_6^{3-} + e^- \rightarrow Fe(CN)_6^{4-}$ on the WE (cathode) and
$Fe(CN)_6^{4-} \rightarrow Fe(CN)_6^{3-} + e^-$ on the CE (anode).

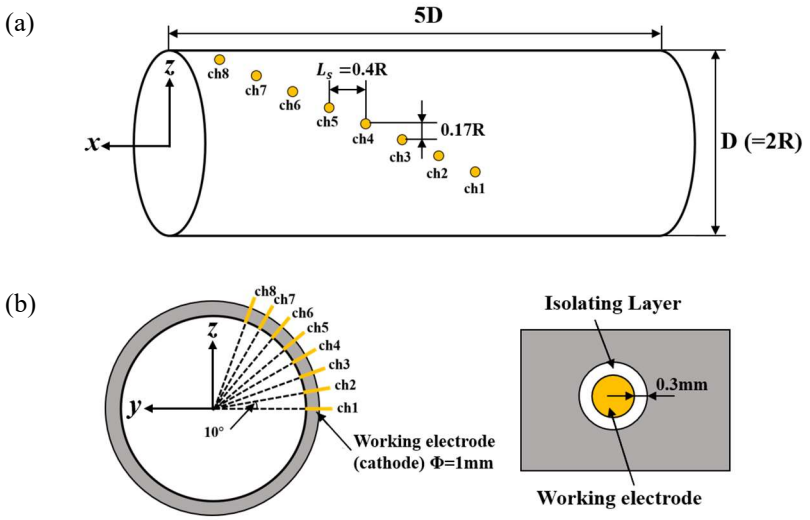

Fig. 2 Point electrode arrangement in the test section: (a) front view of the electrode arrangement and (b) sectional view of the electrode arrangement.

When a voltage is applied to the electrode, a redox reaction occurs on the electrode surface, causing a current. The current increases with the voltage until no further increase occurs at sufficiently high voltages. Under these conditions, the current flowing through the circuit is controlled by the mass transfer rate (Mizushina, 1971). The mass transfer rate $\tilde{k}$ is calculated as

$$\tilde{k} = i/An_eF(c_b - c_w) \tag{1}$$

where c_b is the concentration of the bulk, c_w is the concentration near the wall, A is the surface area of the electrode, n_e is the valence charge of an ion, F is the Faraday constant, and i is the current measured by the three-electrode system using a potentiostat.

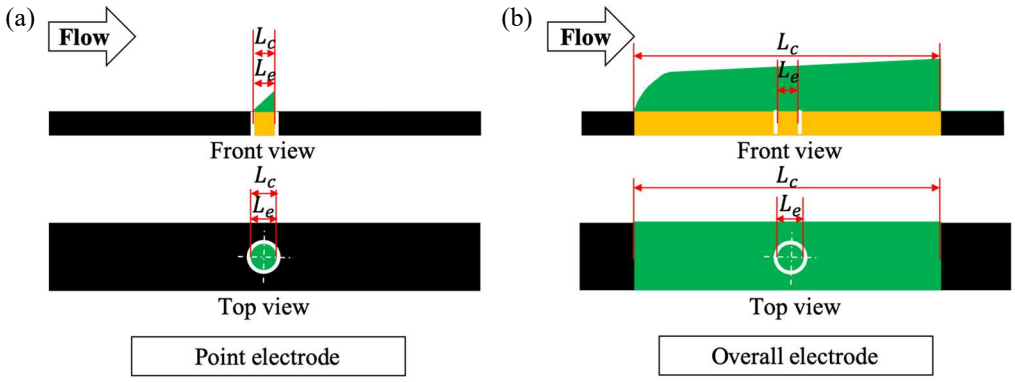

Fig. 3 Schematic view of electrode settings. (a) Normal point electrode ($L_c = L_e$); (b) new designed overall electrode ($L_c \gg L_e$). An image of the concentration boundary layer is shown by green color for each electrode.

[DOI: 10.1299/jfst.2019jfst0013]

2.2 Wall shear stress calculation

In present electrochemical method, the length of concentration boundary layer is defined as L_c, and the length of the electrode for measuring the mass transfer rate is defined as L_e as shown in Fig. 3. The lengths of concentration boundary layers L_c are different for the point electrode and present new designed overall electrode.

For point electrode, the working electrode is the point electrode itself, as shown in Fig.3 (a). The concentration boundary layer develops only on the surface of point electrode with the length L_c. Therefore, the length of the concentration boundary layer equals the length L_e of circular electrode ($L_c = L_e$). For overall electrode, the working electrode is the entire nickel pipe of the test section, as shown in Fig. 3 (b). Then, the concentration boundary layer develops on the entire pipe wall surface of the test section with the length $L_c = 5D$ ($5D$ is length of test section). Therefore, the concentration boundary layer length does not equal the length L_e of circular electrode ($L_c = 5D \neq L_e$). It is noted that the mass transfer rate (or limiting current in Eq. (1)) is measured in the electrode length (L_e) in both the point electrode and overall electrode settings.

There are two methods of calculating the wall shear stress from the mass transfer rate. One method was summarized by Hanratty and Campbell (1983) for the case of a two-dimensional electrode, whose long side is perpendicular to the mean flow direction. If the electrode is small in the flow direction, as shown in Fig. 3 (a), the concentration boundary layer over the point electrode is thin enough to be located under the viscous sublayer and the relationship between the measured mass transfer rate $\bar{k}$ and the velocity gradient $\bar{s}$ satisfies

$$\bar{k} = C\left(\frac{D_f^2 \bar{s}}{L_c}\right)^{1/3} \tag{2}$$

where L_c is the length of concentration boundary layer ($L_c = L_e$ in case of point electrode, associated with the method of Hanratty and Campbell (1983)), D_f is the diffusion coefficient and C is constant. The wall shear stress $\overline{\tau_w}$ is calculated such that $\overline{\tau_w} = \mu\bar{s}$. Therefore, the relationship between the mass transfer rate and the wall shear stress is given as

$$\overline{\tau_w} = \mu\bar{s} = C^{-3}\mu\frac{L_c\bar{k}^3}{D_f^2} \tag{3}$$

In Eq. (3), the coefficient C includes the effect of the electrode shape and size. Hanratty and Campbell (1983) gave one solution for the value of $C = 1.5/(9^{1/3}\Gamma(4/3))$ for predicting the mean wall shear stress according to several assumptions for a two-dimensional electrode; however, based on their method, fluctuations of wall shear stress could not be measured at high frequency nor large amplitude flow.

Another method is to use the Chilton–Colburn analogy, which is an analogy between the heat, momentum, and mass transfer rate. Using the relationship between the momentum and mass transfer rate, we can evaluate the shear stress via a mass transfer measurement (Chilton and Colburn, 1934). The Chilton–Colburn analogy is valid for a fully developed concentration profile in a turbulent flow. Therefore, we designed an overall electrode, where the concentration boundary layer is fully developed on the entire wall surface, as shown in Fig. 3 (b). The concept of an overall electrode is that the same voltage is applied not only to the nickel electrode but also to the nickel pipe of the test section. Therefore, the concentration boundary layer can develop over the entire wall surface of the test section. And the mass transfer rate is measured by the isolated point electrode, as shown in Fig. 3 (b).

The J-factors defined in the Chilton–Colburn analogy need to satisfy

$$j_D = j_h = \frac{C_f}{2} \tag{4}$$

where j_D represents the mass transfer, j_h represents the heat transfer, and C_f represents the fluid friction. Further,

$$j_D = \frac{Sh}{ReSc^{1/3}} \quad , \quad \frac{C_f}{2} = \frac{\overline{\tau_w}}{\rho U_m^2} \tag{5}$$

[DOI: 10.1299/jfst.2019jfst0013]

where Sh is the Sherwood number and Sc is the Schmidt number, and U_m is the cross-section mean velocity. And

$$\frac{Sh}{ReSc^{1/3}} = \frac{\overline{\tau_w}}{\rho U_m^2} \tag{6}$$

$$\overline{\tau_w} = \rho U_m \bar{k} \left(\frac{\nu}{D_f}\right)^{2/3} \tag{7}$$

where ρ is the density of the electrolytic solutions, and ν is the viscosity.

According to the above two methods, the normal point electrode is designed as shown in Fig. 4 (a) so that the voltage is applied only on the small electrode as the cathode; meanwhile, for the overall electrode, as shown in Fig. 4 (b), the entire test section is used as the cathode, loading the same voltage on the test section as on the small electrode. But the mass transfer is measured at isolated local point electrode.

In turbulent flows, the mean wall shear stress $\overline{\tau_w}$ can be predicted from the averaged mass transfer rate $\bar{k}$ by the methods of Hanratty and Campbell (1983) (according to Eq. (3)) and Chilton–Colburn analogy (according to Eq. (7)), as reported by Mizushina (1971) and Lin et al. (1951), respectively. However, the wall shear stress fluctuations are less studied in the experiment due to the difficulties of achieving the undisturbed flow field.

Although based on the method of Hanratty and Campbell (1983), the Eq. (3) can be used for predicting the wall shear stress fluctuations, it has large errors at the high frequency and large amplitude flows. Due to the serious attenuation of the signal over the large length electrode surface, Chilton–Colburn analogy lacks in predicting the wall shear stress fluctuations and has been applied only for measuring the mean wall shear stress with the condition of fully developed concentration boundary layer. However, in present study, with our new designed overall electrode, Chilton–Colburn analogy is applied and studied for the instantaneous wall shear stress measurement by the overall electrode setting, according to Eq. (7).

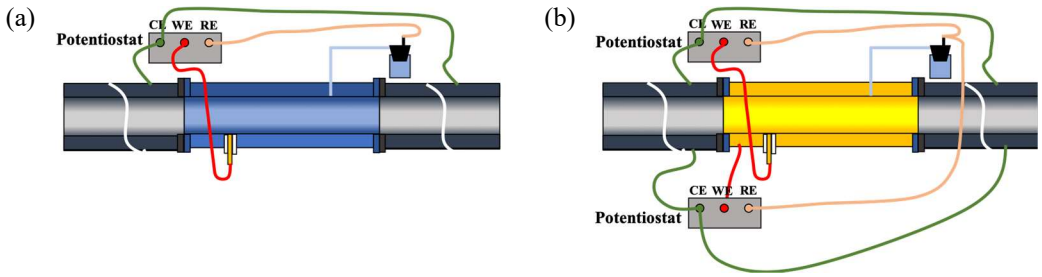

Fig. 4 Schematic view of the connections between the WE, CE, and RE: (a) the point electrode and (b) the overall electrode.

2.3 Experimental setup and conditions

In the present experiment, a potentiostat is used to maintain the potential of the working electrode at a constant level with respect to the reference electrode by adjusting the current at the counter electrode. The potential of the working electrode is maintained at -0.6 V relative to the reference electrode. In the case of the point electrode, as shown in Fig. 4(a), a single potentiostat is used to develop the concentration boundary layer on the surface of the point electrode. However, in the case of the overall electrode, as shown in Fig. 4(b), to create the fully developed concentration boundary layer, the voltage is applied not only to the embedded electrode but also to the entire wall of the test section. Therefore, when using the overall electrode, two potentiostats are used to apply the same voltage on the embedded point electrode and the pipe wall of the test section.

The Reynolds number Re_D, based on the pipe diameter D and the mean cross-sectional velocity U_m, is varied from 25,000 to 65,000, in the present experiment. The friction Reynolds number Re_τ, based on the pipe radius R (D/2) and the friction velocity u_τ, is varied from 700 to 1582. The data are recorded using a 12-bit AD converter with 1 kHz for 30 min (Tong et al., 2018).

3. Results and Discussion

3.1 Mean values of the mass transfer rate and wall shear stress

In previous studies (Son and Hanratty, 1967; Shaw and Hanratty, 1977; Sydberger and Lotz, 1982), the influence of

[DOI: 10.1299/jfst.2019jfst0013]

the length of the concentration boundary layer on the average mass transfer rate was reported. According to the study by Son and Hanratty (1967), the concentration boundary layer, which develops on a small electrode surface, as shown in Fig. 3 (a), is so thin that the diffusion in the flow direction, as well as the curvature of the pipe wall, can be ignored. Under this condition, the relationship between the dimensionless average mass transfer rate $K^+(K^+ = \bar{k}/u_\tau)$ and the concentration boundary layer length L_c^+ $(L_c^+ = L_c u_\tau/\nu)$ is approximated by $K^+ = 0.81(L_c^+)^{-1/3}Sc^{-2/3}$ (Son and Hanratty, 1967). However, when the length L_c^+ increases to a large value, the dimensionless average mass transfer rate K^+ is independent of the concentration boundary layer length L_c^+. Under this condition, when $693 \leq Sc \leq 5070$, K^+ satisfies the empirical equation of $K^+ = 0.0978\,Sc^{-0.716}$ (Shaw and Hanratty, 1977).

The thickness of concentration boundary layer is estimated by $\delta_c = D_f/\bar{k}$ (called Nernst Equation, Hanratty and Campbell, 1983). K^+ is related with δ_c^+ as the relation of $K^+ = (\delta_c^+)^{-1}Sc^{-1}$. According to the previous studies, the concentration boundary layer is fully developed, when K^+ is independent of the concentration boundary layer length L_c^+. For our experiment, with fixed Sc, when δ_c^+ is constant (or the concentration boundary layer is fully developed), the dimensionless mass transfer rate K^+ becomes constant.

Therefore, according to the above two empirical equations, when $Sc = 2100$, the critical length for confirming the fully developed concentration boundary layer is $L_c^+ = 1.76 \times 10^3$, as shown in Fig. 5.

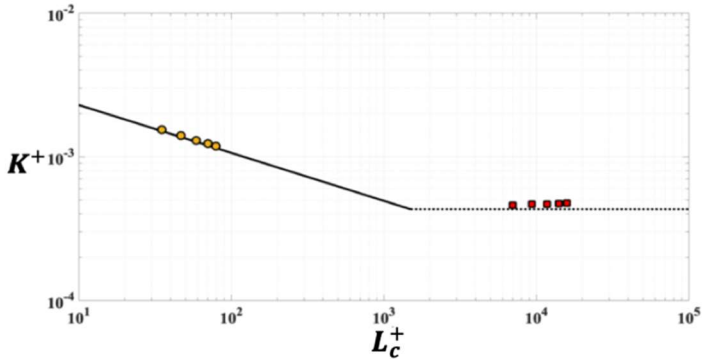

Fig. 5 Dimensionless average mass transfer rate K^+ as a function of the concentration boundary layer length L_c^+. The solid black line indicates $K^+ = 0.81(L_c^+)^{-1/3}Sc^{-2/3}$ (Son and Hanratty, 1967), and the dotted black line indicates $K^+ = 0.0978Sc^{-0.716}$ (Shaw and Hanratty, 1977). The solid yellow circles indicate measurements by the point electrode, and the red squares indicate measurements by the overall electrode.

Figure 5 shows a plot of the dimensionless average mass transfer rate K^+ versus the concentration boundary layer length L_c^+ for the present experiment at $Sc = 2100$. The friction velocity u_τ is obtained using the Blasius equation based on a previous study (Tong et al., 2018). In the point electrode measurement (that is, L_c=L_e), L_c^+ is calculated by the length of circular point electrode with 1mm diameter. The results match with the empirical equation $K^+ = 0.81(L_c^+)^{-1/3}Sc^{-2/3}$ (Son and Hanratty, 1967). In the new designed overall electrode measurement (that is, $L_c = 5D$), L_c^+ is calculated by the length of test section. With traditional concept, the mass transfer rate should be measured by the electrode where concentration boundary is developed. However in the present study, even though the concentration boundary layer is fully developed over the length $L_c = 5D$, the mass transfer rate is measured by a local small point electrode (1mm in diameter) which is isolated in the region where concentration boundary layer is fully developed, as shown in Fig. 3 (b). The results are plotted in Fig. 5 as red square symbols.

Even though the mass transfer rates were measured by small point electrode ($L_e \ll L_c$), they are close to the empirical relation $K^+ = 0.0978Sc^{-0.716}$ (Shaw and Hanratty, 1977). It is indicated that the present new designed overall electrode is available for measuring the average mass transfer rate under fully developed concentration boundary layer.

Figure 6 shows the relationship between the average mass transfer rate and the mean wall shear stress. The vertical axis shows the average mass transfer rate $\bar{k}$ measured by the electrochemical method, and the horizontal axis shows the mean wall shear stress $\overline{\tau_w}$ evaluated via the Blasius equation ($\lambda = 0.3164\,Re^{-0.25}$). The yellow circles with the solid lines and the red squares with the dashed lines show the results for the point electrode (Eq. (3)) and the overall electrode (Eq. (7)), respectively. However, the parameter C in Eq. (3) is different from the value estimated by Hanratty and Campbell (1983); the value of C is corrected according to the shape and size of present electrode. In this study, the

[DOI: 10.1299/jfst.2019jfst0013]

above solid and dashed lines were used as a calibration curve to evaluate the wall shear stress fluctuations of the point and overall electrodes.

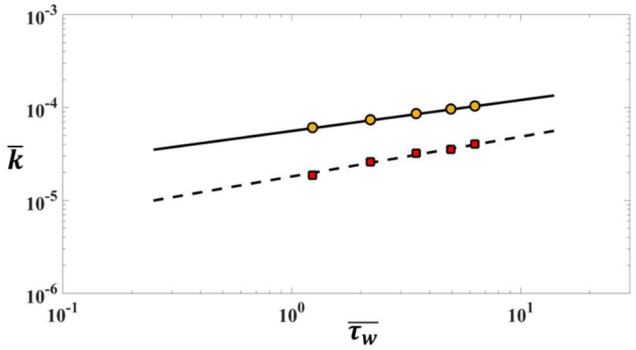

Fig. 6 Calibration curve for the electrochemical method. The solid black line indicates the shear stress estimated by the Blasius equation and transformed into $\bar{k}$ using Eq. (3) with the value of C different from Hanratty and Campbell (1983), corresponding to the point electrode. The dashed black line indicates the shear stress estimated by the Blasius equation and transformed into $\bar{k}$ using Eq. (7), corresponding to the overall electrode. The yellow circles indicate the present experiment with the point electrode, and the red squares indicate the present experiment with the overall electrode.

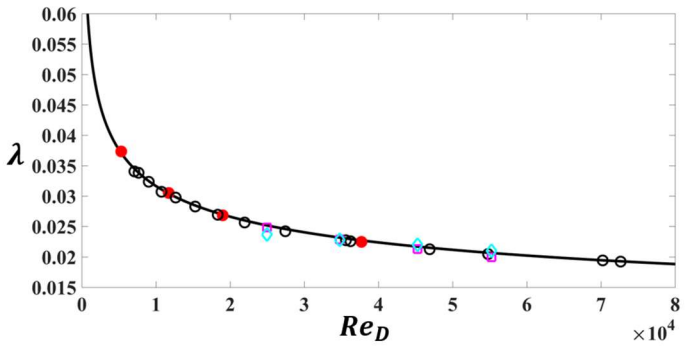

Fig. 7 Friction factor λ as a function of Re_D. The solid black line was derived using the Blasius equation. The solid red circles show the DNS results of Khoury et al. (2013) for a pipe flow. The open circles show the experimental results of Furuichi et al. (2015). The open pink squares show the present experimental results for the point electrode, and the blue diamonds show the present experimental results for the overall electrode.

Due to the different concentration profiles that develop on the point electrode and the overall electrode, the average mass transfer rates measured by these two electrodes are different. However, it is assumed that the mean wall shear stresses calculated from the mass transfer rate by these two electrodes using Eqs. (3) and (7) would be equal under the same flow field. Instead of the wall shear stress, the friction factor λ is used to determine the consistency of the mean wall shear stresses measured by the point and overall electrodes. In Fig. 7, the friction factors, defined as $\lambda = 8u_\tau^2/U_m^2$, are plotted versus the DNS results (Khoury et al., 2013), previous experiments (Furuichi et al., 2015), and the estimations given by the Blasius equation. It can be seen that the present experiment agrees with these friction factors. The mean wall shear stresses calculated according to the Chilton–Colburn analogy and the method of Hanratty and Campbell (1983) have already been presented; however, this is the first time that the mean wall shear stresses predicted by these two methods have been compared under the same turbulent flow conditions. The similar mean values of the wall shear stress measured by the point electrode and the overall electrode, as well as the comparison of the DNS results and the empirical equation, conclude that, even though the concentration boundary profiles develop differently on these two types of electrodes, both can accurately predict the mean wall shear stress.

Adopting the solid line (Eq. (3)) and dashed line (Eq. (7)) in Fig. 6 as calibration curves for measuring the shear stress fluctuations, their statistical features are studied in the next section. Equation (3) has been used to estimate shear stress fluctuations that are low-frequency and large-amplitude oscillations, called pseudo-steady states (Hanratty and Campbell, 1983). However, whether the fluctuations can be measured using Eq. (7) have not been studied. Nor have the

[DOI: 10.1299/jfst.2019jfst0013]

differences in the shear stress fluctuation between a point electrode and an overall electrode been discussed.

3.2 Fluctuations of the mass transfer rate and wall shear stress

3.2.1 Fluctuations of the mass transfer rate

The distribution of fluctuations plays an important role in direct measurement techniques. Probability density functions (PDFs) of the mass transfer rate are shown in Fig. 8 and are compared for the point electrode and the overall electrode. The data are plotted to show the distribution and Reynolds number trends on a linear scale and to emphasize the tail region on a logarithm scale. It is obvious from the results predicted by the overall electrode that the probability of a negative fluctuation occurring at the wall is not zero; the peak is shifted in the negative direction compared to the point electrode, and a higher peak than the distribution of the point electrode is observed. The longer positive tail of the overall electrode PDF indicates much more frequent positive fluctuations, which is consistent with a positive skewness factor. In addition, there is a little Re-number dependency for both the point electrode and the overall electrode when the fluctuation is normalized by its standard deviation. Skewness S and Flatness F are plotted in Fig. 8 (b) against the Reynolds number.

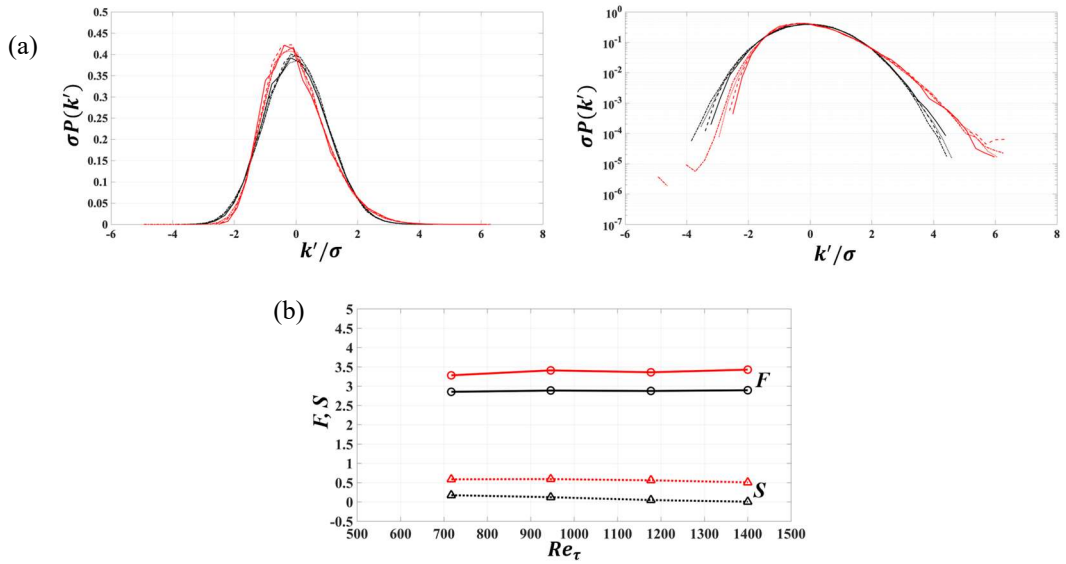

Fig. 8 (a) PDFs at different Reynolds numbers of the mass transfer rate: linear scale (left) and logarithmic scale (right). Red corresponds to the overall electrode and black corresponds to the point electrode. The solid line indicates Re_τ = 700, the dashed line indicates Re_τ = 936, the dotted line indicates Re_τ = 1178, and the dashed-dotted line indicates Re_τ = 1403. (b) Flatness factor and Skewness factor of mass transfer rate. Solid line with open circles is the flatness factor, dotted line with open triangles is the skewness factor. Red indicates the overall electrode; Black indicates the point electrode.

The power spectrum density function was calculated to discuss the difference in the fluctuations between the point electrode and the overall electrode. The one-sided frequency power spectrum density function $E(f)$ is defined as

$$\int_0^{+\infty} E(f)df = 2\int_{-\infty}^{+\infty} E_1(f)df = \sigma^2 \tag{8}$$

where f is the frequency and σ is the standard deviation. Even though a Re-number dependence of the spectrum exists, the differences in the spectra of the point electrode and the overall electrode are independent of the Reynolds number. Figure 9 shows the spectrum at $Re_\tau =$ 1178. It is obvious that the spectrum of the overall electrode is higher than that of the point electrode up to a low frequency near 4 Hz, which corresponds to the large-scale length of 6 R (R is the pipe radius) based on the Taylor's frozen flow hypothesis, where the convection velocity is calculated as $U_c = 10\,u_\tau$ for $y^+ < 5$ (Geng et al., 2015). Then, the spectrum level becomes opposite in the higher frequency region. These differences are likely due to the different frequency responses of the concentration boundary layer for the point electrode and the overall electrode. Further, in the case of the overall electrode, the concentration boundary layer is

[DOI: 10.1299/jfst.2019jfst0013]

fully developed over the entire wall surface; therefore, the local mass transfer fluctuation is affected by the entire concentration boundary layer.

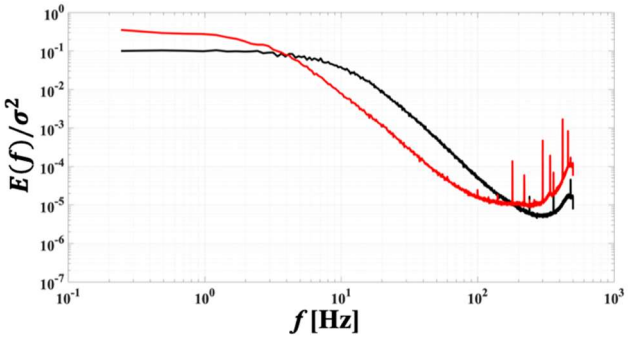

Fig. 9 Comparison of the spectra for the mass transfer rate measured by the point electrode and the overall electrode at Re_τ = 1178. Black corresponds to the point electrode, and red corresponds to the overall electrode.

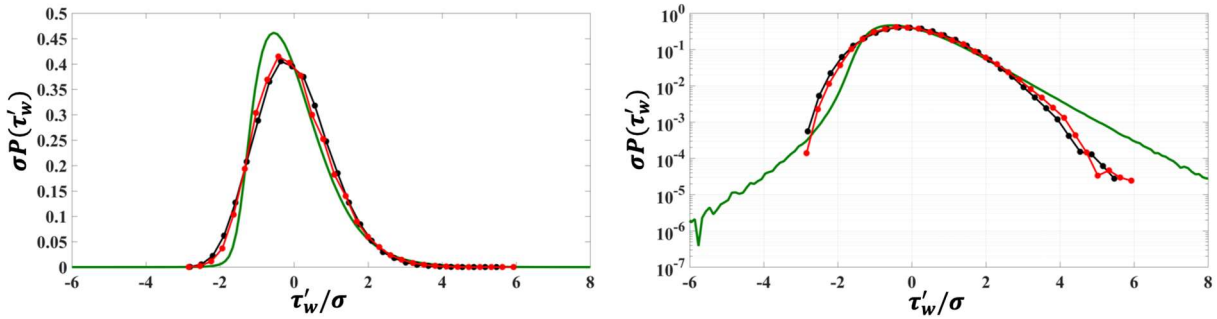

Fig. 10 PDFs of the wall shear stress: linear scale (left) and logarithmic scale (right). The solid green line indicates the DNS results for a channel flow (Mehrez et al., 2019), the black solid circles and line indicate the experimental results for the point electrode, and the red solid circles and line indicate the experimental results for the overall electrode. Re_τ is 1000 for the DNS and 1178 for the experiment.

3.2.2 Fluctuations of the wall shear stress

The fluctuations of the wall shear stress and the velocity are directly related to each other in the vicinity of the wall. Recent studies have revealed a potential influence of large-scale motions on small-scale near-wall structures (Hutchins and Marusic, 2007; Tong et al., 2018), and such an influence could be detected by a local point probe, which corresponds to the small point electrode in the present study. However, accurate wall shear stress fluctuation measurements are difficult due to problems associated with the spatial resolution and the frequency response of the probe (Alfredsson et al., 1988; Kunkel and Marusic, 2003). Figure 10 shows PDFs of the wall shear stress fluctuation normalized by the standard deviation for the present experiment at Re_τ = 1178. It is obvious that the fluctuation distributions predicted by the overall electrode are nearly same as the distributions of the point electrode, as well as those of previous experiments (Wietrzak et al., 1994; Colella et al., 2003). The shear stress fluctuation of the DNS at Re_τ = 1000 in the channel flow is also plotted for comparison (Mehrez et al., 2019). It is clear that the DNS results exhibit a higher peak than the distribution of the present experiment and that the peak of the DNS results is shifted in the negative side compared to the experiment. Such a difference likely originates from the attenuation of the signal over the electrode surface.

The power spectra of the wall shear stresses measured by the point electrode and the overall electrode are also compared. Due to the difference in the concentration boundary layers of the point electrode and the overall electrode, the typical time scales detected by the two electrodes are different. To compare the spectra of the point electrode and the overall electrode, the spectra are normalized with respect to the typical time scales of each electrode. The typical time scale Δt_0 is defined based on the auto-correlation function, as shown in Fig. 11. The auto-correlation function is defined as

[DOI: 10.1299/jfst.2019jfst0013]

$$c(\Delta t) = \langle \tau_w'(t)\tau_w'(t+\Delta t)\rangle/\sigma^2 \tag{9}$$

It is assumed that the correlation coefficient $c(\Delta t)$ decreases as the time interval Δt increases. At a sufficiently large value of Δt_0, the shear stresses $\tau_w'(t)$ and $\tau_w'(t+\Delta t_0)$ are uncorrelated. The typical time scale Δt_0 is given by the zero crossing, which is defined as

$$\Delta t_0 = \Delta t|_{c(\Delta t)=0} \tag{10}$$

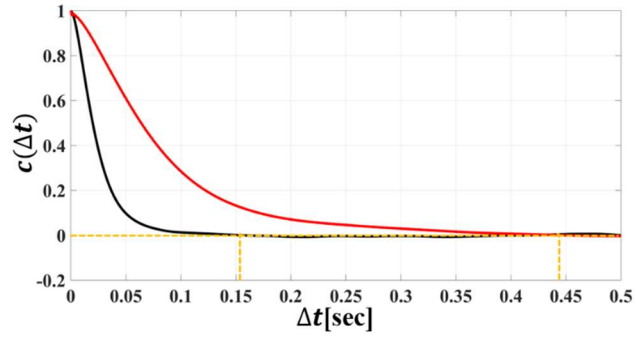

Fig. 11 Auto-correlation curve of the wall shear stress. The black line indicates the point electrode with the zero crossing at $\Delta t_0 = 0.15$ s. The red line indicates the overall electrode with the zero crossing at $\Delta t_0 = 0.44$ s.

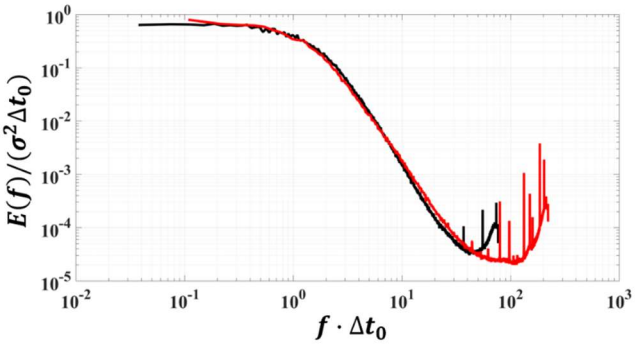

Fig. 12 Power spectra of the wall shear stress normalized by the typical time. The solid black line is measured by the point electrode, and the solid red line is measured by the overall electrode where $Re_\tau = 1178$.

Figure 12 shows the spectra for a comparison of the point electrode and the overall electrode. It is clear that the spectra of the two electrodes match very well over the entire frequency region. The same statistics between point electrode and overall electrode are consistent with the result of PDF. These results conclude that, for the electrochemical method, both Eq. (3) and Eq. (7) can be used to calculate the instantaneous wall shear stress and give similar shear stress fluctuation distributions.

Note that the consistency of fluctuation statistics between the point electrode and the overall electrode is realized well in the case of a canonical flow field, such as a circular tube, channel, and boundary layer. However, the consistency is not always satisfied in a complex turbulent flow field where the flow is not stationary, or when the concentration boundary layer is not two dimensional.

3.2.3 Spatial resolution effect in the experiment

In previous studies, the differences in the spectra have been discussed (Sreenivasan and Antonia, 1977; Keith et al., 1991; Wei and Willmarth, 1989) and have been attributed to the poor frequency response and spatial resolution of the measurement probe. Since the PDFs are different between DNS (Mehrez et al., 2019) and present experiment, we suppose this difference is due to the finite area of electrode in the experiment, which attenuates the spatial resolution, and is due to the non-uniform concentration (or not two-dimensional) boundary layer developed on the circular electrode surface. In order to evaluate the effect of spatial resolution on the present measurement by small point

[DOI: 10.1299/jfst.2019jfst0013]

electrode, DNS data are used in the following.

The shear stress fluctuations of DNS are averaged over some area and PDF and spectrum are calculated. These results, in turn, are used to discuss how PDF and spectrum varies depending on the size of averaged area.

In the experiment, the dimensionless surface area (normalized by the viscous scale) of the point electrode is $A^+ = 1.09 \times 10^4$. The space-averaged areas of the DNS are simple square shapes and $A^+ = 3.89 \times 10^3$, 1.10×10^4, 3.17×10^4 and 3.52×10^6.

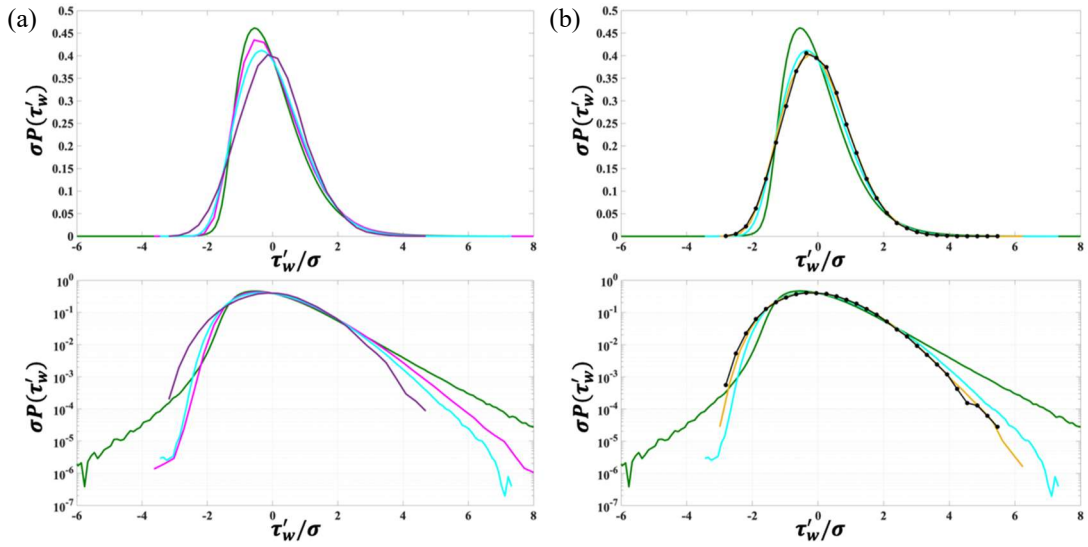

Fig. 13 PDFs of the wall shear stress: linear scale (above) and logarithmic scale (below). The solid green line indicates the DNS results for a channel flow (Mehrez et al., 2019). (a) Comparison of PDFs among the averaged DNS areas: pink indicates $A^+ = 3.89 \times 10^3$, blue indicates $A^+ = 1.10 \times 10^4$, and purple indicates 3.52×10^6. (b) Comparison of PDFs among the averaged DNS results and the experiment: the solid blue line indicates DNS with $A^+ = 1.10 \times 10^4$, yellow line indicate $A^+ = 3.17 \times 10^4$ and the dotted black line indicates the point electrode with $A^+ = 1.09 \times 10^4$. Re_τ is 1000 for the DNS and 1178 for the experiment.

With the help of DNS data, we analyze how PDF changes with increasing averaged area. Figure 13 (a) shows the comparison of PDFs among different averaged areas. The averaged areas are $A^+ = 3.89 \times 10^3, 1.1 \times 10^4$ and 3.52×10^6. It is clear to see that with increasing averaged area, the peak of the PDF is towards to the positive side, approaching to zero and its value decreases. Especially, the positive tail part region becomes small with increasing averaged area. From these results it is concluded that the positive high amplitude fluctuations are attenuated with increasing the averaged areas.

Figure 13 (b) shows the comparison among DNS ($A^+ = 1.1 \times 10^4$) and experiment ($A^+ = 1.09 \times 10^4$). It indicates that with the similar spatial averaged area, the PDF of experiment is different with DNS, especially the positive tail part region is smaller than DNS. The better agreement is obtained by the averaged area of $A^+ = 3.17 \times 10^4$, which is approximately three times larger than the point electrode area of experiment.

This area difference is attributed to the electrode shape. In the experiment, electrode shape is circle, but the space averaged area of DNS data is square. However, the main issue of discussion is the attenuation of PDF, which is confirmed with the help of DNS data. In the further experiment, the smaller electrode size may increase the accuracy of shear stress measurement in present system.

A comparison of the spectra is made using the wavenumber spectra, which is defined as

$$\int_0^{+\infty} \phi(k_x) dk_x = 2 \int_{-\infty}^{+\infty} \phi_1(k_x) dk_x = \sigma^2 \tag{11}$$

where k_x is the streamwise wavenumber. The convection velocity U_c, which is used to calculate the wavenumber from the frequency ($k_x = 2\pi f / U_c$) in the present experiment, is given by $U_c = 10u_\tau$ for $y^+ < 5$ (Geng et al., 2015). Figure 14 shows the comparison of spectra among the DNS data. The streamwise wave number is normalized by pipe

[DOI: 10.1299/jfst.2019jfst0013]

radius R in experiment and channel half height h in DNS. The spectra are normalized by standard deviations. DNS data are averaged in square shape over the area $A^+ = 1.1 \times 10^4$ and 3.17×10^4. It can be seen from Fig. 14 that with increasing averaged area of DNS, the high wave-number spectrum fails to be displayed. The finite area average decreases the spatial resolution and loses the detection of the high frequency fluctuations. The spectrum of experiment is different from that of DNS especially in high wave-number region. A better agreement is confirmed in the low wave-number regions around 20Hz for the spectrum of averaged area $A^+ = 3.17 \times 10^4$.

The inconsistent space-averaged area between DNS and experiment is due to the edge effect of the circular electrode, which was mentioned before. From the comparison of spectra among space-averaged DNSs and experiment, it is concluded that the frequency resolution of experiment is not enough because the finite size of electrode.

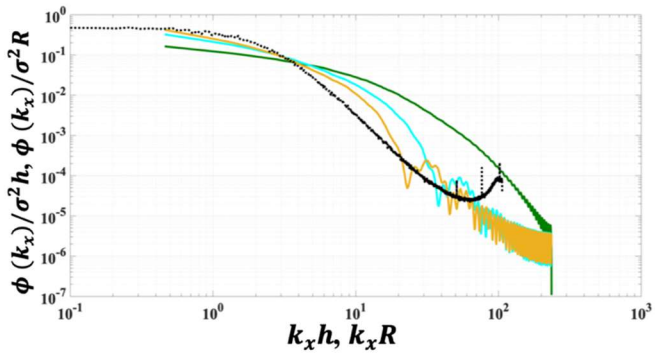

Fig. 14 Wavenumber spectra of the wall shear stress. The solid green line indicates the DNS results for a channel flow (Mehrez et al., 2019), the solid blue line indicates the DNS results with $A^+ = 1.10 \times 10^4$, yellow line indicates $A^+ = 3.17 \times 10^4$. The dotted black line indicates the point electrode with $A^+ = 1.09 \times 10^4$ of experiment. Re_τ is 1000 for the DNS and 1178 for the experiment.

From the PDF and spectral statistical approaches, similar distributions of the wall shear stress fluctuations are obtained via the Chilton–Colburn analogy and the method of Hanratty and Campbell (1983) because a sufficient agreement of the statistics between the overall electrode and the point electrode is confirmed. However, when the spatial resolution is taken into consideration, compared to the DNS results, it appears from the PDFs and spectrum that the present experiment cannot accurately predict large amplitude and high frequency of wall shear stress fluctuations; this difference between experiments and DNSs has been reported in previous studies (Hu et al., 2006).

3.3 Two-point correlations of the local mass transfer rate

In previous study (Tong et al., 2018), it was discussed how large-scale structures in log region affect the near wall region via the simultaneous measurement of flow field and mass transfer rate. By comparing the two-point correlations of the streamwise velocity fluctuation and mass transfer fluctuation, the mass transfer rate at the wall is observed to be related to the large-scale velocity structures in the log region. Therefore, in previous study, it is concluded that the footprint of large-scale turbulent structures in the log region affects the near-wall region, enhancing the mass transfer rate. However, the streamwise motions of large-scale structure in log region and mass transfer rate in the near wall region were not analyzed. In present study, we directly compare the convection velocity of mass transfer rate and the velocity structures in the near wall region by way of two-point correlation and DNS data.

The statistical properties of the structure associated with the mass transfer fluctuation k' between adjacent electrode positions are studied via the two-point correlation. The two-point correlation coefficient is defined as

$$R(\Delta t) = \langle k'_m(t) k'_n(t + \Delta t) \rangle / (\sigma_m \sigma_n) \qquad , m = 1, 2 \ldots 7; n = m+1 \tag{12}$$

where lower subscripts m and n indicate the electrode channel (see Fig. 2), and their standard deviations are expressed by σ.

Figure 15 shows the correlation coefficient versus the time lag at different Reynolds numbers Re_D. It is obvious that the value of the peak of the correlation coefficient increases with Re_D and that the time lag Δt at the peak decreases.

[DOI: 10.1299/jfst.2019jfst0013]

According to the previous study (Tong et al., 2018), the mass transfer rate is influenced by the footprints of the large-scale turbulent streamwise velocity structures observed in the log region. The spanwise width of the large-scale velocity structures close to the wall is approximately 0.2 R (Tong et al., 2018), which is of the same order as the spanwise distance of 0.17 R of the present electrode positions (as indicated in Fig. 2 (a)). Due to this, we suspect that the two adjacent electrodes are affected by the same large-scale turbulent velocity structures; the very short time lags Δt_p of the peak may indicate the streamwise motion of footprint of large-scale structures. For this verification, the streamwise convection velocity is estimated based on the two-point correlation of mass transfer rate, and is compared with DNS estimation (Geng et al., 2015).

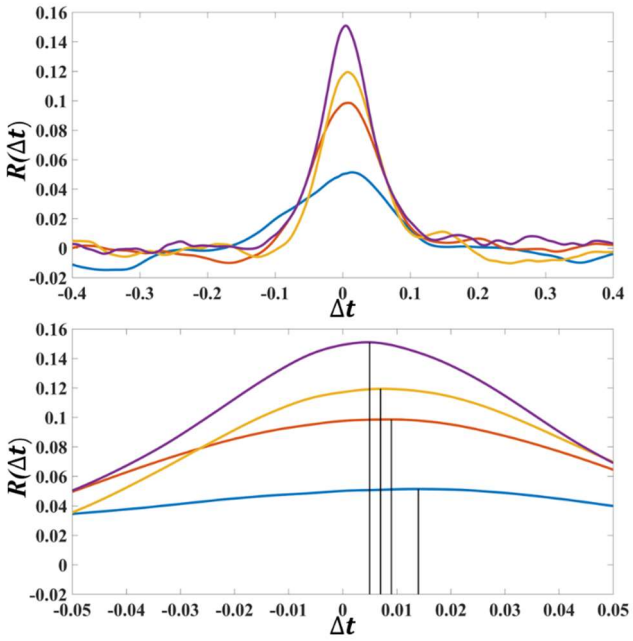

Fig. 15 Two-point correlation of the mass transfer rate as a function of the time lag: full plot (above) and partial enlargement (below). Blue indicates Re_D = 25,000, red indicates Re_D = 35,000, yellow indicates Re_D = 45,000, and purple indicates Re_D = 55,000. The maximum time lag Δt_p is indicated by the solid vertical line for each Re number: Re_D = 25,000, $\Delta t_p = 0.014$ s; Re_D = 35,000, $\Delta t_p = 0.009$ s; Re_D = 45,000, $\Delta t_p = 0.007$ s; and Re_D = 55,000, $\Delta t_p = 0.005$ s.

The streamwise convection velocity U_s, estimated by the mass transfer, is calculated as

$$U_s = L_s/\Delta t_p \tag{13}$$

where L_s (=0.4 R) is the streamwise distance between two adjacent point electrodes. In previous DNS studies of channel flows (Geng et al., 2015), the streamwise convection velocity U_c has been estimated as a constant such that $U_c = 10u_\tau$ for $y^+ < 5$. A comparison between the DNS and the present experiment is shown in Fig. 16 (a). It indicates that the streamwise convection velocity U_s, estimated by k', has the similar trend of Re-number dependency as the convection velocity U_c of DNS estimation. And U_s is approximately two times larger than the DNS estimation (Geng et al., 2015), as shown in Fig. 16 (b). This might be because the electrode size (d = 1 mm) is relatively large compared to the spanwise distance of the electrodes (0.17 R = 6.8 mm). And also the quantitative difference in Fig. 16 (b) might be due to the spanwise meandering of the large-scale structures (Hutchins and Marusic, 2007). Based on the two-point correlation of mass transfer fluctuation, the convection velocity U_s, estimated by mass transfer rate, has the similar features with the convection velocity U_c of DNS estimation. This confirms that the present two adjacent electrodes are indeed included in one structure. And the similar Re-number dependency confirms that large-scale structure, observed in log-region, do affect the mass transfer rate in the near wall region by its footprint, and the footprint has the similar traveling speed with mass transfer rate.

[DOI: 10.1299/jfst.2019jfst0013]

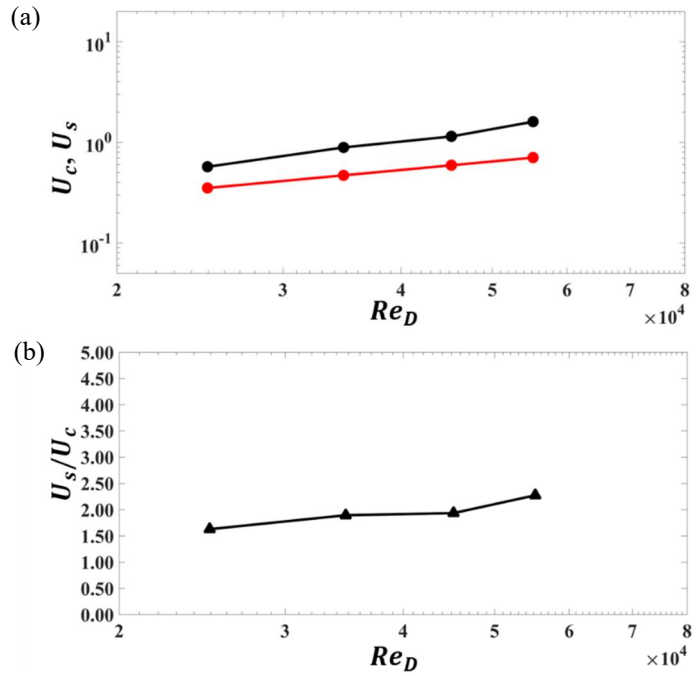

Fig. 16 (a) Convection velocities versus Re_D: the solid black circles indicate values estimated from the present experiment (U_s) and the solid red circles indicate values estimated from the DNS results using the relationship $U_c = 10u_\tau$ for $y^+ < 5$ (Geng et al., 2015). (b) Ratio between the experimental and DNS velocities.

4. Conclusions

The dimensionless average mass transfer K^+ versus the length of concentration boundary layer L_c^+ was compared to previous studies (Son and Hanratty, 1967; Shaw and Hanratty, 1977) to evaluate the feasibility of present new designed overall electrode and to verify the accuracy of the point electrode. It is found that the point electrode makes a good agreement with empirical equation $K^+ = 0.81(L^+)^{-1/3}Sc^{-2/3}$ (Son and Hanratty, 1967), and the mass transfer rate measured by new designed overall electrode is similar with the empirical relation $K^+ = 0.0978Sc^{-0.716}$ (Shaw and Hanratty, 1977). From these results, it is concluded that the present new designed overall electrode can be applied for the electrochemical measurement.

The mean wall shear stresses measured by the point and overall electrodes are compared via their friction factors. The present results match well with the Blasius equation and DNS results (Khoury et al., 2013), as well as previous experiments (Furuichi et al., 2015), which conclude that both the point electrode and the overall electrode can accurately predict the mean wall shear stress.

The relation between the average mass transfer rate and the mean wall shear stress is used as a calibration curve to evaluate the wall shear stress fluctuations of the point and overall electrodes. A sufficient agreement with both previous studies and the empirical values indicated the feasibility of the present experimental data measured by the point and overall electrodes and that these data could be used to analyze the wall shear stress.

The fluctuations of the wall shear stress measured by the point and overall electrodes are compared using their PDFs and spectra. The shear stress fluctuations measured by the point and overall electrodes have the same statistical features. Therefore, we conclude that the Chilton–Colburn analogy can predict the statistical features of the shear stress fluctuation. However, such an agreement may only be satisfied in the case of a canonical flow field, such as a circular tube, channel, or boundary layer.

Due to the finite area of electrode of present experiment, the attenuation of signal over the electrode surface cannot be neglected. To evaluate the spatial resolution effect on the present fluctuation measurement in experiment, the DNS of a channel flow (Mehrez et al., 2019) is used to discuss the effect of the spatial resolution of the experiment. From the comparison of PDFs and spectra of shear stress fluctuation with those of DNS data, it is found that the spatial and time frequency resolution in experiment are nonidentical with DNS. We conclude that these differences are due to the finite size of electrode.

[DOI: 10.1299/jfst.2019jfst0013]

Finally, the two-point correlation of the mass transfer rate between two adjacent point electrode positions is examined to discuss the streamwise convection velocity based on the Taylor's frozen hypothesis and is compared to the DNS estimation in a channel flow (Geng et al., 2015). The convection velocity calculated by the mass transfer is slightly larger than the measured velocity; however, both velocities display a similar Re-number dependency. Based on our previous study (Tong et al., 2018), it is concluded that the large-scale structures do affect the mass transfer rate in the near wall region by its footprint and it moves at the similar velocity with mass transfer structure.

Acknowledgment

We appreciate the experimental support by Mr. T. Hayashi and the constructive criticism of the manuscript by Mr. K. Bhatt through the research. This work is partially supported by "Nagoya University High Performance Computing Research Project for Joint Computational Science" in Japan. Financial support from Japan Society for the Promotion of Science (B) Grant No. 20360083 is gratefully acknowledged.

References

Alfredsson, P. H., Johansson, A. V., Haritonidis, J. H. and Eckelmann, H., The fluctuating wall-shear stress and the velocity field in the viscous sublayer, The Physics of fluids Vol.31, No.5 (1988), pp.1026-1033.

Bard, A. J., Faulkner, L. R., Leddy, J. and Zoski, C. G., Electrochemical methods: fundamentals and applications, Vol. 2. New York: wiley (1980).

Chilton, T. H. and Colburn, A. P., Mass transfer (absorption) coefficients prediction from data on heat transfer and fluid friction, Industrial & engineering chemistry Vol.26, No.11 (1934), pp.1183-1187.

Chin, D. T. and Hsueh, K. L., An analysis using the Chilton—Colburn analogy for mass transfer to a flat surface from an unsubmerged impinging jet, Electrochimica acta Vol.31, No.5 (1986), pp.561-564.

Colella, K. J. and Keith, W. L., Measurements and scaling of wall shear stress fluctuations, Experiments in fluids Vol.34, No.2 (2003), pp.253-260.

El Khoury, G. K., Schlatter, P., Noorani, A., Fischer, P. F., Brethouwer, G. and Johansson, A. V., Direct numerical simulation of turbulent pipe flow at moderately high Reynolds numbers, Flow, turbulence and combustion Vol.91, No.3 (2013), pp.475-495.

Fortuna, G. and Hanratty, T. J., Frequency response of the boundary layer on wall transfer probes, International Journal of Heat and Mass Transfer Vol.14, No.9 (1971), pp.1499-1507.

Francis H. Clauser., Turbulent boundary layers in adverse pressure gradients, Journal of the Aeronautical Sciences Vol.21, No.2 (1954), pp.91-108.

Furuichi, N., Terao, Y., Wada, Y. and Tsuji, Y., Friction factor and mean velocity profile for pipe flow at high Reynolds numbers, Physics of Fluids Vol.27, No.9 (2015), Paper No. 095108.

Geng, C., He, G., Wang, Y., Xu, C., Lozano-Durán, A. and Wallace, J. M., Taylor's hypothesis in turbulent channel flow considered using a transport equation analysis, Physics of Fluids Vol.27, No.2 (2015), Paper No.025111.

Hanratty, T.J. and Campbell, J.A., Measurement of wall shear stress. In: Goldstein, R.J. (Ed.), Mechanics Measurements. Hemisphere Publishing Co. (1983), pp.559–615.

Hu, Z., Morfey, C. L. and Sandham, N. D., Wall pressure and shear stress spectra from direct simulations of channel flow, AIAA journal Vol.44, No.7 (2006), pp.1541-1549.

Hutchins, N. and Marusic, I., Evidence of very long meandering features in the logarithmic region of turbulent boundary layers, Journal of Fluid Mechanics Vol.579 (2007), pp.1–28.

Hutchins, N., Monty, J. P., Ganapathisubramani, B., Ng, H. C. H., and Marusic, I., Three-dimensional conditional structure of a high-Reynolds-number turbulent boundary layer, Journal of Fluid Mechanics Vol.673 (2011), pp. 255-285.

Keith, W. L. and ENNETT, J. C., Low-frequency spectra of the wall shear stress and wall pressure in a turbulent boundary layer, AIAA journal Vol.29, No.4 (1991), pp.526-530.

Kunkel, G. J. and Marusic, I., An approximate amplitude attenuation correction for hot-film shear stress sensors, Experiments in fluids Vol.34, No.2 (2003), pp.285–290.

Lin, C. S., Denton, E. B., Gaskill, H. S. and Putnam, G. L., Diffusion-controlled electrode reactions, Industrial &

[DOI: 10.1299/jfst.2019jfst0013]

Engineering Chemistry Vol.43, No.9 (1951), pp.2136-2143.
Marusic, I. and Heuer, W. D., Reynolds number invariance of the structure inclination angle in wall turbulence, Physical review letters Vol.99, No.11 (2007), 114504.
Mehrez, A., Philip, J., Yamamoto, Y. and Tsuji, Y., Pressure and spanwise velocity fluctuations in turbulent channel flows: Logarithmic behavior of moments and coherent structures, Physical Review Fluids Vol.4, No.4 (2019), Paper No.044601.
Mitchell, J. E. and Hanratty, T. J., A study of turbulence at a wall using an electrochemical wall shear-stress meter, Journal of fluid mechanics Vol.26, No.1 (1966), pp.199-221.
Mizushina, T., The electrochemical method in transport phenomena, Advances in heat transfer Vol.7, Elsevier (1971) pp.87-161.
Örlü, R. and Schlatter, P., On the fluctuating wall-shear stress in zero pressure-gradient turbulent boundary layer flows, Physics of fluids Vol.23, No.2 (2011), Paper No.021704.
Patel, V. C., Calibration of the Preston tube and limitations on its use in pressure gradients, Journal of Fluid Mechanics Vol.23, No.1 (1965), pp.185-208.
Sandborn, V. A., Evaluation of the time dependent surface shear stress in turbulent flows, American Society of Mechanical Engineers (1979).
Schlatter, P. and Örlü, R. Quantifying the interaction between large and small scales in wall-bounded turbulent flows: a note of caution, Physics of fluids Vol.22, No.5 (2010), Paper No.051704.
Shan, F., Characteristics of flow field and wall mass transfer rates downstream of a circular squared-edged orifice plate in a round pipe, Doctoral dissertation. Department of Energy Engineering and Science Graduate School of Engineering, Nagoya University, (2014).
Shaw, D. A. and Hanratty, T. J., Turbulent mass transfer rates to a wall for large Schmidt numbers, AIChE Journal Vol.23, No.1 (1977), pp.28-37.
Silverman, D. C., Conditions for similarity of mass-transfer coefficients and fluid shear stresses between the rotating cylinder electrode and pipe, Corrosion Vol.61, No.6 (Jun 2005), pp.515-518.
Son, J. S. and Hanratty, T. J., Limiting relation for the eddy diffusivity close to a wall, AIChE Journal Vol.13, No.4 (1967), pp.689-696.
Sreenivasan, K. R. and Antonia, R. A., Properties of wall shear stress fluctuations in a turbulent duct flow, Journal of Applied Mechanics Vol.44, No.3 (1977), pp.389-395.
Sumer, B. M., Arnskov, M. M., Christiansen, N. and Jørgensen, F. E., Two-component hot-film probe for measurements of wall shear stress, Experiments in Fluids Vol.15, No.6 (1993), pp.380-384.
Sydberger, T. and Lotz, U., Relation between mass transfer and corrosion in a turbulent pipe flow, Journal of the Electrochemical Society Vol.129, No.2 (1982), pp.276-283.
Tong, T., Tsuneyoshi, T., Ito, T. and Tsuji, Y., Instantaneous mass transfer measurement and its relation to large-scale structures in pipe flow, International Journal of Heat and Fluid Flow Vol.71 (2018), pp.160-169.
Wei, T. and Willmarth, W. W., Reynolds-number effects on the structure of a turbulent channel flow, Journal of Fluid Mechanics Vol.204 (1989), pp.57-95.
White, F. M., Viscous Fluid Flow (McGraw-Hill Mechanical Engineering). Vol. 3. New York: McGraw-Hill (2005).
Wietrzak, A. and Lueptow, R. M., Wall shear stress and velocity in a turbulent axisymmetric boundary layer, Journal of Fluid Mechanics Vol.259 (1994), pp.191-218.
Winter, K. G., An outline of the techniques available for the measurement of skin friction in turbulent boundary layers, Progress in aerospace sciences Vol.18 (1979), pp.1-57.

[DOI: 10.1299/jfst.2019jfst0013]